Nitrogen incorporation in graphene nanowalls via plasma processes : experiments and simulations Author information

Andrea Jagodar, Johannes Berndt, Erik von Wahl, Thomas Strunskus, Thomas Lecas, Eva Kovacevic, Pascal Brault

Title:

Nitrogen incorporation in graphene nanowalls via plasma processes : experiments and simulations

Author information:

Andrea Jagodar[1], Johannes Berndt[1], Erik von Wahl[1], Thomas Strunskus[2], Thomas Lecas[1], Eva Kovacevic[1], Pascal Brault[1]

[1]GREMI CNRS-University of Orleans, 14 rue d'Issoudun, 45067 Orleans Cedex 2, France

[2] Institute for Materials Science, Christian Albrechts University Kiel, Kaiserstr, 2, 24143 Kiel, Germany

*Corresponding author: andrea.jagodar@univ-orleans.fr

Abstract

The interest in doped and functionalized graphene nanomaterials for various applications is growing due to the development of new and simple production and treatment methods. Amongst the techniques used to treat graphene nanomaterials dry methods like plasmas or ion beams are of particular interest. In this work a low temperature plasma technique is used to incorporate nitrogen atoms into the carbon network of graphene sheets. In order to gain a better understanding of such processes material analysis techniques (NEXAFS and XPS) were combined with the results coming from molecular dynamics simulations and plasma know-how. The results show that the plasma post treatment of graphene nanowalls can be regarded as a balance between vacancy formation, functionalization, doping and crosslinking. Moreover, MD simulations provided insight into fundamental mechanisms like the formation of different bonds due to the interaction of the surface with different kind of species with variable kinetic energy. This can help to improve different types of doping/functionalization techniques using energetic species: the study reveals for example the role of N2+ species, the kinetics of

vacancy formations depending on type and energy of the species, the formation of amines or graphitic nitrogen, and the role of impurities such as NHx species.

Keywords

Graphene, Graphene nanowalls, Plasma post-treatment, Nitrogen incorporation, molecular dynamics simulations, NEXAFS spectroscopy, XPS spectroscopy

1. Introduction

The interest in novel carbonaceous materials with large effective surface areas, high conductivity and stability, and low cost has been growing in recent decades stimulated by new demands e.g. super capacitors and sensors [1, 2] . In particular 2D materials with high electrical conductivity have attracted a great amount of interest in this context and especially graphene: doped and functionalized graphene, horizontally or vertically grown graphene as well as graphene in the form of free standing flakes [3].

Although graphene and graphene like materials are rather inert surfaces, they can be modified to add specific, tailored surface functionalities or to change their mechanical or electrical properties. There are several methods that can be employed for the doping and functionalization of graphene, for example, certain chemical methods [4], UV light treatment [5], ion beams or plasma processes (gas discharges) [6].

The incorporation of nitrogen atoms in a graphene lattice is often of a special interest, since this process changes the lattice symmetry and affects mechanical properties as well as thermal and electrical conductivity of the graphene (how the properties are changed, depends on the doping level) [7]. The effect of the nitrogen incorporation on the material properties of graphene naturally depends on how exactly the N-atoms are incorporated in the carbon network, i.e. whether one has for example graphitic-N, pyridinic-N or pyrrolic-N. Graphitic-N, for example, in which the nitrogen is linked to 3 carbon atoms, can be regarded as the most promising nitrogen configuration for adjusting the electrical properties since the N-doping effect is strong without significantly changing the original structure. It was reported that graphitic-N plays an eminent role in various applications such as in

electrodes for oxygen reduction reactions (ORR) [8 –10], molecular sensors [11], water oxidations [12] and electromagnetic devices [13]. It was shown that nitrogen plasmas can introduce graphitic N (quaternary nitrogen) in the basal plane or pyrrolic groups at the edges of the CNWs structure, depending on the plasma conditions [14]. The selective incorporation of e.g. graphitic nitrogen by plasma processes is still a large challenge and a better understanding of the plasma induced processes and changes is needed.

Amongst various methods for the treatment of graphene and graphene nanowalls as well as the incorporation of foreign atoms, nitrogen plasma based treatments offer some specific advantages. They are regarded as environmental friendly processes and they are already widely used in research and development as well as in industrial processes, as for example in car industry or for biomedical applications [15, 16].

There are different types of plasmas used nowadays for the functionalization and doping of materials, ranging from arc devices to low temperature plasmas and from atmospheric to low pressure systems. In this work a low power and low pressure RF plasmas is used. This type of plasma is a typical example for a technological low temperature plasma. Low temperature plasmas are far away from thermal equilibrium and are characterized by rather low gas temperatures (which are usually close to room temperature) and by relatively small ionization degrees. This kind of plasma is therefore well suited for the modification of surfaces, as for example doping and functionalization of graphene like materials, since they allow surface treatments without causing excessive damage to the surfaces. However, the interaction of surfaces with plasmas is a rather complex process which involves even for “simple” gases, as nitrogen, different species impinging at the surfaces with different kinetic energies. The aim of this work is to give an insight into this process and thus enable the control of the plasma post-treatment of graphene sheets/walls. This will be achieved by combining experimental observations (materials and plasmas) with molecular dynamics simulations (MD). The MD simulations will provide insight into fundamental mechanisms like the formation of different kinds of bonds due to the interaction of the surface with different kinds of species having different kinetic energies. This is important for applications as given earlier in [8]–[12], [17]. Recent progress in building force fields [18] opened the

door to rigorously include reactivity and bond orders in these simulations. The MD results will be compared with the results coming from the material analysis such as Near Edge X-ray-absorption fine-structure spectroscopy (NEXAFS) and X ray photoelectron spectroscopy (XPS). Surface analysis with high precision methods like NEXAFS can give an insight in even the slightest changes in the bonding situation at surfaces, and is very applicable for materials like graphene.

2. Material and methods

2.1. Preparation and analysis of materials

The treatment of CNWs was performed in a specially designed low power low pressure capacitively coupled RF plasma previously described in [19]. The experiments were operated at room temperature, with a nitrogen flow of 20 sccm during 30 min. The total gas pressure during the process was set to 0.1 mbar, and the reactor was pumped until the same vacuum (10^{-6} mbar) before each process with a turbomolecular pump. The input power ranged between 3 to 10 W and the example given here is obtained at 8 W. The discharge was carried out between two stainless steel parallel plate electrodes with a diameter of 12 cm and a distance of 5.5 cm between them. Capacitively coupled plasmas of this type are widely used to modify the surface topography or the surface chemistry of materials [6]. A specific feature of this type of discharge concerns the formation of a DC self-bias voltage on the powered electrode, which leads to an additional acceleration of the positive ions in the direction of this electrode. The value of the mean kinetic energy of positive ions arriving at the powered electrode can be therefore considerably higher than the corresponding value at the grounded electrode [14].

The carbon nanowalls used in the experiments were produced by another RF discharge on a heated, grounded electrode. The detailed scheme of the experimental setup, and also the process of synthesis of CNWs has been presented in our previous studies [20], [21].

The material itself (before and after treatment) was analyzed by a High Resolution Scanning Electron microscope (SEM) Zeiss Supra 40.

The chemical bonding situation has been analyzed by means of XPS and Near Edge X-ray fine structure analysis-spectroscopy (NEXFAS) using the HE-SGM beamline at BEESY II synchrotron. NEXAFS data were obtained on the C K-edge and N K-edge, in the partial electron yield (PEY) mode, using a home built double channel plate detector. The energy resolution was ≈0.40 eV for the C K edge, and 0.60 eV for the N K-edge. The raw NEXAFS spectra were normalized to the incident photon flux and corrected for the beam line transmission by division through a spectrum of a clean, freshly sputtered Au sample (for more details on spectra treatment, see [22]–[26]. Here, for the sake of simplicity, presented XPS and NEXAFS spectra are obtained at the angle of 45°. The angle of 45° is close to the magic angle which should be at 52° for the 82% polarization degree at the HE-SGM beamline. XPS spectra were analyzed using Casa XPS software by curve fitting method including background fitting [27].

2.2. Reactive Molecular dynamics simulations of N_x and NH_x interactions with nanowalls

Molecular dynamics (MD) simulations are used in this work to simulate the interaction of a graphene sheet with nitrogen based species with variable kinetic energies. A ReaxFF force field has been chosen [27] for describing many body interactions of nitrogen based species with graphene sheets. ReaxFF force fields have the advantage of allowing bond breaking/formation taking into account the bond orders. The bond orders in ReaxFF are calculated as a function of interatomic distances. Moreover, partial charges are evaluated at each time step [18]. Simulations were run using LAMMPS software [29]–[31].

A 3D periodic simulation box used in the calculations has a size of 4.3 x 4.9 x 6.0 nm^3. A graphene sheet is located at the center of the box and 200 molecules of interest (N, N_2, NH, NH_2, and NH_3, respectively) are randomly placed apart each side of the sheet. Periodic boundaries mean that escaping molecules on one side appears on the other. This simulates a stationary gas phase interacting on each side of the nanowalls. Fig 2 represents a snapshot of the simulation box, with the example of N_2 molecules.

For the simulations, we used the following parameters: a pre-formed carbon sheet surface (graphene) is thermostated at 300 K using a Langevin thermostat with a 100 fs damping time, while N, N_2, NH, NH_2 or NH_3 species have variable vapor temperature. So the initial velocities at such temperatures are selected in a Maxwell-Boltzmann distribution. The simulation time is 250 ps with a time step of 0.25 fs, i.e. 10^6 time steps overall. The simulations were run separately for each possible species issued from the N_2 plasma, such as N, N_2.

The choice of species (i.e. N, N_2, NH, NH_2 or NH_3) is based on previous observations and on the experimental analysis of plasma species obtained by means of mass spectroscopy [32]–[34].

Each run is carried out for kinetic energies in the range of 1-10 eV with a step of 1 eV. Two additional runs are performed for 15 and 20 eV. Thus, the type of defect formation will be analyzed with regard to the nature of the species and their kinetic energy.

3. Results

The results are divided in two parts. The analysis of the deposited and treated CNWs will be presented in the first part, followed by the presentation of the results coming from the MD simulations.

3.1. Material analysis

The morphological changes of the CNW samples due to the nitrogen plasma treatment were studied by electron microscopy. Fig 2 a) shows a SEM image of a reference sample, i.e. an image of CNWs prior to the nitrogen plasma treatment. The SEM images confirm the typical morphology of pristine CNWs [14], [20], [35]. Fig 2 b) and c) show SEM images of CNW samples after the plasma treatment. Fig 2 b) shows a sample that was placed on the grounded electrode, Fig 2 c) a sample that was placed on the powered electrode during the plasma treatment. A comparison between these images shows that the plasma treatment causes only small changes in the morphology of the CNWs. Slight differences can be observed for the CNWs placed on the powered electrode (slightly etched surface).

The results of these observations were supported by means of XPS and NEXAFS analysis. The XPS survey spectra for the reference sample and the nitrogen plasma treated CNWs are plotted in Fig 3.

The measurements show that the nitrogen plasma treatment of the CNWs is accompanied by a certain amount of oxygen incorporation into the material. This oxygen probably originates from the saturation of dangling bonds created by the plasma. These bonds react with oxygen after the samples are exposed to atmosphere or with eventual impurities in the plasma itself. [25], [36]

The chemical structure of the nitrogen plasma treated CNWs can be seen from XPS C1s in Fig 3 a) and b). The main peak fitted in the C 1s region is centered at 284.4 eV which is assigned to sp^2 carbon atoms bound to carbon or hydrogen atoms. Peaks centered at higher binding energies are assigned to sp^3 carbon atoms bound to other carbons or hydrogen atoms (285.0 eV), carbon bound to nitrogen or singly bound to oxygen (peaks at 285.7 and 286.6 eV), carbon in carbonyl groups (287.6 eV) and carbon in carboxylate groups (289.0 eV). The nitrogen content in the sample placed on the grounded electrode is 2 at.%, and on the powered electrode 3 at.%. The oxygen content in the sample placed on the grounded electrode is 5 at.% and 9 at.% for the powered. The nitrogen peak is fitted by components attributed to graphitic (401.5 eV), pyrrollic (400.6 eV), amine (399.7 eV), pyridinic (398.8 eV), nitrile (398.0 eV). Usually in literature [37], [38] only graphitic, pyrrollic and pyridinic peaks are fitted, but our MD simulations suggest that this is not sufficient. Hence, additional peaks for nitrile and amine have to be considered. The oxygen peak (fig 3g and h) is fitted by three components: C=O (carbonyl) for the lowest binding energy, -COOH (basal-plane hydroxyls) for the medium and C-OH (chemisorbed oxygen and water) for the highest [39], [40]. Adsorbed water is usually not present at room temperature in the XPS because it will desorb under UHV conditions. Thus these will be covalently bound oxygen species.

More details are visible from Fig 4, which shows the NEXAFS C K-edge spectrum of the reference sample and the spectra of the treated samples (placed on the grounded and powered electrode respectively). The reference spectrum shows sharp C 1s $\rightarrow \pi^*$ resonances at 285.2 eV ("graphene fingerprint" region, C1). A second dominant feature is double-structured resonance around 292 eV (C4 and C5), which corresponds to C 1s $\rightarrow \sigma^*$. This double-structured resonance has an excitonic origin

(at 292.12eV) and it is followed by band-like contributions (broad peaks in the range of 293–320 eV) [25]. They are typical for graphene like structures and show that the carbon nanowalls essentially consist of intact graphene layers with only few defects. Around 287.6 eV (C2), very weak broad features are measured, which are often discussed to be related to defects, or to interlayer states in low symmetry regions of the Brillouin zone [26], [41], [42].

A comparison of the C K-edge of the reference and the nitrogen plasma treated CNWs at the "fingerprint" region shows the decrease of the sp^2 C-C bonds at 285.2 eV (C1) for nitrogen treated CNWs. This decrease is more pronounced for the sample which was placed on the powered electrode and less pronounced for the sample which was on the grounded electrode.

For the nitrogen plasma treated CNWs we observe the rise of a new peak at around 288.4 eV (C3) which is in our case connected with the introduction of impurities in the carbon network: oxygen and nitrogen presence in the material as seen in the XPS spectra. This region is known as a region where peaks originating from bonds with foreign atoms appear after doping or functionalization [25], [26]. The intensity of this peak is stronger for the CNWs placed on the powered electrode (connected with lower intensity of π^*) which implies greater changes in the original structure.

The analysis of the excitonic peak shows that the graphene-like structure is better preserved for the sample placed on the grounded electrode.

The NEXAFS N K-edge spectra of the nitrogen plasma treated samples (Fig 4) show the presence of three peaks in the region between 389 eV and 401 eV and the broad σ^* signal starting at 405.0 eV. The shoulder at 398.7 eV corresponds to pyridinic species (N1), the peak at 399.59 eV corresponds to nitrile and pyrrolic bonds (N2), and 400.9 eV originates from graphitic nitrogen with contribution of molecular nitrogen and/or presence of NH_x groups (N3) [14], [22], [43]–[45]. It is important to emphasize that no signal could be detected in the N K-edge of the reference CNWs sample.

3.2. MD analysis

The MD simulations were carried out to explain the obtained NEXAFS spectra and especially the origin of the most important types of defects resulting from the interaction of the graphene sheet with the plasma. The MD analysis is performed by calculating the number and type of bonds formed for the case when N, N2, NH, NH2 and NH3 species with different energies interact with a graphene sheet. Varying energies is intended to include effects of ions which are treated as fast neutrals in MD simulations. This is justified if ions are neutralized close to the interacting surfaces, i.e. until the extended graphene sheet is able to transfer free electrons to the incoming ions. [46]

Fig 6 shows the graphene sheet modifications at the end of the simulations, i.e. after 106 time steps (250 ps) at different kinetic energies of incoming species and for all types of species.

The snapshots show that species with highest kinetic energies (15 and 20 eV) are generating a great amount of structural damage on the graphene sheet, for which the structure is almost completely lost. For the smallest energies of N and N2 species (5eV), the structural integrity of the graphene network remains rather intact. However, for all energies we can also observe the incorporation of N atoms into the graphene network. The following types of stable nitrogen bonds in the graphene sheet have been observed in the simulations: on top nitrogen, bridge out of plane nitrogen, graphitic nitrogen (quaternary nitrogen), pyridinic nitrogen, on top NH, amine and other complicated configurations as illustrated in Fig 7 (Avogadro and VMD software were used for post-processing of MD simulations [47]–[50]) .

Figure 8 shows the number of the different types of defects found at the end of each simulation for the different types of species. The most abundant types are on top N and amines followed by bridge N which is an intermediate structure between on top N and pyridinic / graphitic-N. Pyridinic and graphitic-N structures are found in smaller amounts in the simulation results.

In addition to the incorporation of N species into the graphene network the simulations reveal the formation of several types of vacancies or intrinsic defects characterized by the existence of non-hexagonal rings encircled by hexagonal rings

[51]. During the simulations, the occurrence of various vacancy defects such as Stone Wales defects or single vacancy defects was observed.

A careful inspection of the MD simulation results based on a frame-by-frame analysis shows that the formation of vacancies is crucial for the incorporation of N species into the carbon network. The simulations reveal that vacancies occur during the first collisions of N species with the graphene sheet (in the first frames of the simulation). These vacancies act then as active sites for subsequent reactions with further incoming N species.

This is illustrated in Fig 9 which shows the formation of graphitic-N and pyridinic-N due to the interaction of the graphene sheet with N atoms of 2 eV. The starting point is a vacancy created by the impact of an N atom on the graphene sheet. As already mentioned, vacancies play the role of active sites i.e. in this case another N atom binds to the *vacancy-edge* C atom, and initially creates a top defect (on top N) and then a bridge NN position.

This leads then either to the formation of pyridinic-N or to the formation of graphitic-N. Once nitrogen has been incorporated in the hexagonal lattice in pyridinic or graphitic form we can observe some instabilities: after the incorporation of the N atom in frame 12, a change between the graphitic and the pyridinic form can be seen from frame 14 to 84, in Fig 9. After frame 84, the graphitic form stays stable until the end of the simulation (frame 3000). Similar trends are found in the N2 and NHx simulations. The only difference between Nx simulations and NHx simulations is that usually on neighbor vacancy edge C atoms, H atoms are connected as on top H.

4. Discussion

Unlike experiments performed in plasmas, MD simulations can be used to study the interaction of specific molecules, radicals or atoms with the substrate. A detailed frame-by-frame analysis of the MD simulations can yield information about the reaction mechanisms leading to the formation of specific configurations. MD simulations are therefore an important tool that can help to predict, to understand, and to control the outcome of plasma experiments.

Comparing the NEXAFS and XPS spectra (in particular the N K-edge, which gives more details on particular incorporation of nitrogen then C K edge) with MD results, it is possible to make the following statements:

- The MD simulations clearly confirm the importance of the kinetic energy of the species impinging onto the graphene sheet. In particular, the bombardment of the graphene sheet with high energy ions can lead to substantial material damages (Fig 6). This is in agreement with the experimental results which show that plasma – CNW interactions depend on the position of the CNWs in the chamber i.e. whether they are placed on the GE or PE. Due to the self-bias formed at the PE, the samples are exposed to an ion flux which is characterized by higher kinetic energies. The electron microscope images (Fig 2) confirm that the surface morphology of the CNWs placed on the PE is different from the surface morphology of the pristine samples. The surface morphology of the samples placed on the GE on the other hand shows no obvious differences compared to the untreated samples. This is confirmed by the NEXAFS and XPS results (C K-edge) which show that for the sample which was on the PE the graphene like structure is slightly damaged what can be observed by the decrease of the sp2 C-C species and the increase of defects.

- The frame-by-frame analysis of the MD results showed that the formation of defects is a crucial step for the incorporation of foreign atoms into the graphene network.

- As consequence: The exact amount of nitrogen doping/functionalization and oxygen incorporation depends on the kinetic energy of the species arriving at the substrates (i.e. in our case on the position of the sample –PE or GE). As mentioned before, a decrease in sp2 C-C species and an increase of defects can be the pre-stage for the incorporation of nitrogen and oxygen in the material. XPS C1s fitting provides, in addition, information about the atomic percentage of new, foreign atoms. For nitrogen it is 2 at.% in the GE sample, and 3 at.% for sample on the powered electrode. Oxygen, which is

not visible in the untreated, pristine sample, rises in the GE sample to 5 at.% and to 9 at.% for the PE sample. The presence of oxygen can be explained in a few ways: open bonds that are not saturated during the plasma treatment, are saturated after the exposure to air, it can also come from possible impurities in the plasma, and finally a small contribution can come from the underlying oxidized substrate surface (aluminum, nickel, Si wafer).

- The general influence of the nitrogen incorporation in the carbon lattice can be noticed by changes in the peak C3 in NEXAFS (the rise of the new peaks at around 288.39 eV) or 285.7 and 286.6 eV peaks in C 1s of XPS.

- The N1 peak in NEXAFS, the π* band with the lowest energy (Fig 5), originates from pyridine, which has nitrogen bound to two carbon neighbors and appears to be the least intense among the π* peaks in all presented cases as well as in the cases presented in literature [14]. The same type of bonds was observed in XPS at 398.8 eV (Fig 3 e and f). The number of pyridine like sites in the MD simulations is increasing above a threshold energy of about 4 eV for each species and gains significance at higher energies.

- The N2 peak (399.5 eV) in NEXAFS, originates theoretically from nitrile and pyrrolic species. In the literature, nitrile observed in NEXAFS for this category of materials, is explained as a N≡C structure at the basal graphite, which is expected to have on top orientation and be more prominent at high N concentration in material [14], [22], [52]. In some publications [53] this peak is correlated with N_2^+ ion reactions with the graphene lattice (which is in our case the dominant ion). In XPS spectra, these bonds are visible at 400.6 eV for pyrrolic and and 398 eV for nitrile. MD results show on top nitrogen which can be bound by single, double and triple bonds. MD confirms the assupmtions about N_2^+: although we can get on top N for all types of species, the number is the highest for N_2 plasma species. Pyrrolic N was not observed in MD simulations as a stable bonding situation.

- The N3 peak from NEXAFS N K-edge (401.0 eV) originates from substituted nitrogen in the hexagonal graphitic structure, graphitic-N. However, this is also the region where amine groups can be detected [26], usually observed in literature at the right wing of such peaks as N3 in Fig 4. In XPS we observe 401.5 eV for graphitic and 399.7 eV for amine. MD confirms the presence of such multiple bonds: we got all 3 kinds of assumed functionalization: on top NH, amino, and the most promising doping situation, graphitic-N.

- Following the results of the MD simulations, graphitic and pyridinic-N do not appear at the same time and in the same order for N and N_2 simulations: in the case of N, which is more reactive, graphitic-N is created earlier than pyridinic-N, and in the case of N_2 simulations pyridinic-N is created earlier then the graphitic form. The threshold energy for the creation of graphitic and pyridinic N is lower for N species than for N_2 species. This is consitent with the higher reactivity of N species compared to N_2. Considering N_2^+ being the dominant ion in the plasma this explains the strong pyridinc contribution in the XPS analysis.

- The simulations revealed that in the beginning of the formation of graphitic-N, the nitrogen atom is embedded in a vacancy in a bridge position or as pyridinic-N.

- One more suprising result is the observation of the amine peak in XPS: this shows the important role of plasma impurities in the graphene doping. The role of NH_x species is confirmed as very important and the MD study can also be used for ammonia plasmas.

- The number of defects depends on the number of collisions, and the number of collisions depends on the plasma density. The model presented herein is a simplified view because the impact of each species on the graphene sheet is treated separately, and each species is assumed to have the same density. In plasmas, different species act simultaneously and the ratio of the fluxes

of different species will depend on the experimental details. However, this can also be seen as a model that can be used as a base to emulate effects of different plasmas and ions beams.

5. Conclusion

The incorporation of foreign atoms (as e.g. nitrogen) into the carbon network of graphene sheets opens new possibilities for applications ranging from supercapacitors to sensors. In particular, dry processes like ion beams, CVD techniques or plasma-based methods are uniquely suited to dope or functionalize graphene materials. In order to tailor the outcome of the doping process information obtained from high precision surface diagnostics as XPS and NEXAFS is combined in this work with information about the RF capacitively coupled nitrogen plasma, and the results coming from molecular dynamics simulations.

Briefly, the MD simulations reveal that vacancies occur during the first collisions of N species with the graphene sheet. These vacancies act then as active sites for subsequent reactions with further incoming N species resulting in C-N bond formation. The exact amount of nitrogen doping/functionalization and oxygen incorporation depends strongly on the kinetic energy of the species arriving at the substrates (i.e. in our case on the position of the sample – PE or GE). MD confirms the importance of N_2^+ ions for the formation of on top N. Pyrrolic N was neither observed in MD nor in material analysis as a stable, and consequently, a dominant bonding situation. MD also confirms the presence of multiple bonds as they are observed by XPS or NEXAS. All 3 kinds of expected functionalities are present and are predicted to appear: on top NH, amines, and the most promising doping situation, graphitic-N. Moreover, graphitic and pyridinic-N do not appear at the same time and in the same order in the simulations of N and N_2 species: in the case of N, which is more reactive, graphitic-N is created earlier than pyridinic-N, vice versa for N_2 species, as we expected from the experimental point of view (higher reactivity of N species). MD also showed the importance of NH_x species (in the presented experimental work they were only present as impurities) for the formation of vacancies and amines. These MD predictions can be thus used for a broader number of processes containing nitrogen or NH_x species (ion beams or plasmas).

Acknowledgements

The work was performed under the framework of PEGASUS (Plasma Enabled and Graphene Allowed Synthesis of Unique Nanostructures) project, funded by the European Union's Horizon Research and Innovation Program under grant agreement No. 766894. The authors would also like to acknowledge the financial support provided by the French Research Agency through the project Plasma-Bond under grant agreement ANR--17-CE08-0018. The authors want to thank HZB for the allocation of synchrotron radiation beamtime at Bessy II. This project has received funding from the European Union's Horizon 2020 research and innovation programme under grant agreement No 730872 (Nr. 18207084-ST and 18207393-ST).

References:

[1] F. Yi, H. Ren, J. Shan, X. Sun, D. Wei, and Z. Liu, "Wearable energy sources based on 2D materials," *Chem. Soc. Rev.*, vol. 47, no. 9, pp. 3152–3188, 2018, doi: 10.1039/C7CS00849J.

[2] P. Dyakonov *et al.*, "Carbon nanowalls as a platform for biological SERS studies," *Sci Rep*, vol. 7, no. 1, p. 13352, Dec. 2017, doi: 10.1038/s41598-017-13087-8.

[3] E. Tatarova *et al.*, "Towards large-scale in free-standing graphene and N-graphene sheets," *Sci Rep*, vol. 7, no. 1, p. 10175, Dec. 2017, doi: 10.1038/s41598-017-10810-3.

[4] D. W. Boukhvalov and M. I. Katsnelson, "Chemical functionalization of graphene," *J. Phys.: Condens. Matter*, vol. 21, no. 34, p. 344205, Aug. 2009, doi: 10.1088/0953-8984/21/34/344205.

[5] X. Liu, E. K. Lee, and J. H. Oh, "Graphene-Ruthenium Complex Hybrid Photodetectors with Ultrahigh Photoresponsivity," *Small*, vol. 10, no. 18, pp. 3700–3706, Sep. 2014, doi: 10.1002/smll.201400403.

[6] J. Berndt, H. Acid, E. Kovacevic, C. Cachoncinlle, Th. Strunskus, and L. Boufendi, "Deposition and tuning of nanostructured hydrocarbon deposits:

From superhydrophobic to superhydrophilic and back," *Journal of Applied Physics*, vol. 113, no. 6, p. 063302, Feb. 2013, doi: 10.1063/1.4789949.

[7] P. T. Araujo, M. Terrones, and M. S. Dresselhaus, "Defects and impurities in graphene-like materials," *Materials Today*, vol. 15, no. 3, pp. 98–109, Mar. 2012, doi: 10.1016/S1369-7021(12)70045-7.

[8] J. Li *et al.*, "Direct Transformation from Graphitic C_3N_4 to Nitrogen-Doped Graphene: An Efficient Metal-Free Electrocatalyst for Oxygen Reduction Reaction," *ACS Appl. Mater. Interfaces*, vol. 7, no. 35, pp. 19626–19634, Sep. 2015, doi: 10.1021/acsami.5b03845.

[9] T. Sharifi, G. Hu, X. Jia, and T. Wågberg, "Formation of Active Sites for Oxygen Reduction Reactions by Transformation of Nitrogen Functionalities in Nitrogen-Doped Carbon Nanotubes," *ACS Nano*, vol. 6, no. 10, pp. 8904–8912, Oct. 2012, doi: 10.1021/nn302906r.

[10] D. Geng *et al.*, "High oxygen-reduction activity and durability of nitrogen-doped graphene," *Energy Environ. Sci.*, vol. 4, no. 3, p. 760, 2011, doi: 10.1039/c0ee00326c.

[11] R. Lv *et al.*, "Nitrogen-doped graphene: beyond single substitution and enhanced molecular sensing," *Sci Rep*, vol. 2, no. 1, p. 586, Dec. 2012, doi: 10.1038/srep00586.

[12] W. He, C. Jiang, J. Wang, and L. Lu, "High-Rate Oxygen Electroreduction over Graphitic-N Species Exposed on 3D Hierarchically Porous Nitrogen-Doped Carbons," *Angew. Chem. Int. Ed.*, vol. 53, no. 36, pp. 9503–9507, Sep. 2014, doi: 10.1002/anie.201404333.

[13] A. Zabet-Khosousi *et al.*, "Segregation of Sublattice Domains in Nitrogen-Doped Graphene," *J. Am. Chem. Soc.*, vol. 136, no. 4, pp. 1391–1397, Jan. 2014, doi: 10.1021/ja408463g.

[14] N. M. Santhosh *et al.*, "N-Graphene Nanowalls via Plasma Nitrogen Incorporation and Substitution: The Experimental Evidence," *Nano-Micro Lett.*, vol. 12, no. 1, p. 53, Feb. 2020, doi: 10.1007/s40820-020-0395-5.

[15] D. B. Graves, "Plasma processing," *IEEE Trans. Plasma Sci.*, vol. 22, no. 1, pp. 31–42, Feb. 1994, doi: 10.1109/27.281547.

[16] B. Graham, "Technological plasmas," *Phys. World*, vol. 14, no. 3, pp. 31–36, Mar. 2001, doi: 10.1088/2058-7058/14/3/28.

[17] O. L. Li and T. Ishizaki, “Development, Challenges, and Prospects of Carbon-Based Electrode for Lithium-Air Batteries,” in *Emerging Materials for Energy Conversion and Storage*, Elsevier, 2018, pp. 115–152. doi: 10.1016/B978-0-12-813794-9.00004-1.

[18] T. P. Senftle *et al.*, “The ReaxFF reactive force-field: development, applications and future directions,” *npj Comput Mater*, vol. 2, no. 1, p. 15011, Nov. 2016, doi: 10.1038/npjcompumats.2015.11.

[19] C. Pattyn, E. Kovacevic, S. Hussain, A. Dias, T. Lecas, and J. Berndt, “Nanoparticle formation in a low pressure argon/aniline RF plasma,” *Appl. Phys. Lett.*, vol. 112, no. 1, p. 013102, Jan. 2018, doi: 10.1063/1.5019926.

[20] S. Hussain *et al.*, “Low-temperature low-power PECVD synthesis of vertically aligned graphene,” *Nanotechnology*, vol. 31, no. 39, p. 395604, Jul. 2020, doi: 10.1088/1361-6528/ab9b4a.

[21] T. Labbaye *et al.*, “Enhancement of catalytic effect for CNT growth at low temperature by PECVD,” *Applied Surface Science*, vol. 453, pp. 436–441, Sep. 2018, doi: 10.1016/j.apsusc.2018.05.059.

[22] E. Kovačević *et al.*, “Formation and material analysis of plasma polymerized carbon nitride nanoparticles,” *Journal of Applied Physics*, vol. 105, no. 10, p. 104910, May 2009, doi: 10.1063/1.3129318.

[23] T. Labbaye *et al.*, “*In situ* Raman spectroscopy for growth monitoring of vertically aligned multiwall carbon nanotubes in plasma reactor,” *Appl. Phys. Lett.*, vol. 105, no. 21, p. 213109, Nov. 2014, doi: 10.1063/1.4902915.

[24] A. Nefedov and C. Wöll, “Advanced Applications of NEXAFS Spectroscopy for Functionalized Surfaces,” in *Surface Science Techniques*, vol. 51, G. Bracco and B. Holst, Eds. Berlin, Heidelberg: Springer Berlin Heidelberg, 2013, pp. 277–303. doi: 10.1007/978-3-642-34243-1_10.

[25] C. Ehlert, W. E. S. Unger, and P. Saalfrank, “C K-edge NEXAFS spectra of graphene with physical and chemical defects: a study based on density functional theory,” *Phys. Chem. Chem. Phys.*, vol. 16, no. 27, pp. 14083–14095, 2014, doi: 10.1039/C4CP01106F.

[26] J. Stöhr, *NEXAFS Spectroscopy*, vol. 25. Berlin, Heidelberg: Springer Berlin Heidelberg, 1992. doi: 10.1007/978-3-662-02853-7.

[27] V. Kuznetsov *et al.*, “Neutron spectroscopy study of the diffusivity of hydrogen in MoS_2,” *Phys. Chem. Chem. Phys.*, vol. 23, no. 13, pp. 7961–7973, 2021, doi: 10.1039/D0CP05136E.

[28] L. Zhang, A. C. T. van Duin, S. V. Zybin, and W. A. Goddard III, “Thermal Decomposition of Hydrazines from Reactive Dynamics Using the ReaxFF Reactive Force Field,” *J. Phys. Chem. B*, vol. 113, no. 31, pp. 10770–10778, Aug. 2009, doi: 10.1021/jp900194d.

[29] S. Plimpton, “Fast Parallel Algorithms for Short-Range Molecular Dynamics,” *Journal of Computational Physics*, vol. 117, no. 1, pp. 1–19, Mar. 1995, doi: 10.1006/jcph.1995.1039.

[30] H. M. Aktulga, J. C. Fogarty, S. A. Pandit, and A. Y. Grama, “Parallel reactive molecular dynamics: Numerical methods and algorithmic techniques,” *Parallel Computing*, vol. 38, no. 4–5, pp. 245–259, Apr. 2012, doi: 10.1016/j.parco.2011.08.005.

[31] “LAMMPS Molecular Dynamics Simulator.” https://www.lammps.org/ (accessed Aug. 23, 2021).

[32] L. L. Alves *et al.*, “Capacitively coupled radio-frequency discharges in nitrogen at low pressures,” *Plasma Sources Sci. Technol.*, vol. 21, no. 4, p. 045008, Aug. 2012, doi: 10.1088/0963-0252/21/4/045008.

[33] C. Pattyn, “Procédés pour le développement de bio-capteurs à partir de surfaces de carbone nanostructurées obtenues par plasma froid,” These de doctorat, Orléans, 2018. Accessed: Aug. 22, 2021. [Online]. Available: https://www.theses.fr/2018ORLE2063

[34] M. Jiménez-Redondo *et al.*, “N_2 –H_2 capacitively coupled radio-frequency discharges at low pressure: II. Modeling results: the relevance of plasma-surface interaction,” *Plasma Sources Sci. Technol.*, vol. 29, no. 8, p. 085023, Sep. 2020, doi: 10.1088/1361-6595/ab9b1b.

[35] M. Hiramatsu, K. Shiji, H. Amano, and M. Hori, “Fabrication of vertically aligned carbon nanowalls using capacitively coupled plasma-enhanced chemical vapor deposition assisted by hydrogen radical injection,” *Appl. Phys. Lett.*, vol. 84, no. 23, pp. 4708–4710, Jun. 2004, doi: 10.1063/1.1762702.

[36] H. Biederman, *Plasma Polymer Films*. PUBLISHED BY IMPERIAL COLLEGE PRESS AND DISTRIBUTED BY WORLD SCIENTIFIC PUBLISHING CO., 2004. doi: 10.1142/p336.

[37] N. Bundaleska *et al.*, “Large-scale synthesis of free-standing N-doped graphene using microwave plasma,” *Sci Rep*, vol. 8, no. 1, p. 12595, Dec. 2018, doi: 10.1038/s41598-018-30870-3.

[38] A. Vesel, R. Zaplotnik, G. Primc, and M. Mozetič, “A Review of Strategies for the Synthesis of N-Doped Graphene-Like Materials,” *Nanomaterials*, vol. 10, no. 11, p. 2286, Nov. 2020, doi: 10.3390/nano10112286.

[39] M. K. Rabchinskii *et al.*, “Modulating nitrogen species via N-doping and post annealing of graphene derivatives: XPS and XAS examination,” *Carbon*, vol. 182, pp. 593–604, Sep. 2021, doi: 10.1016/j.carbon.2021.06.057.

[40] Z. Xing *et al.*, “One-pot hydrothermal synthesis of Nitrogen-doped graphene as high-performance anode materials for lithium ion batteries,” *Sci Rep*, vol. 6, no. 1, p. 26146, May 2016, doi: 10.1038/srep26146.

[41] D. A. Fischer, R. M. Wentzcovitch, R. G. Carr, A. Continenza, and A. J. Freeman, “Graphitic interlayer states: A carbon *K* near-edge x-ray-absorption fine-structure study,” *Phys. Rev. B*, vol. 44, no. 3, pp. 1427–1429, Jul. 1991, doi: 10.1103/PhysRevB.44.1427.

[42] R. A. Rosenberg, P. J. Love, and V. Rehn, “Polarization-dependent C(*K*) near-edge x-ray-absorption fine structure of graphite,” *Phys. Rev. B*, vol. 33, no. 6, pp. 4034–4037, Mar. 1986, doi: 10.1103/PhysRevB.33.4034.

[43] N. Hellgren *et al.*, “Electronic structure of carbon nitride thin films studied by X-ray spectroscopy techniques,” *Thin Solid Films*, vol. 471, no. 1–2, pp. 19–34, Jan. 2005, doi: 10.1016/j.tsf.2004.03.027.

[44] S. C. Ray *et al.*, “Electronic properties of a-CNx thin films: An x-ray-absorption and photoemission spectroscopy study,” *Journal of Applied Physics*, vol. 98, no. 3, p. 033708, Aug. 2005, doi: 10.1063/1.1994933.

[45] K.-J. Kim *et al.*, “Surface property change of graphene using nitrogen ion,” *J. Phys.: Condens. Matter*, vol. 22, no. 4, p. 045005, Feb. 2010, doi: 10.1088/0953-8984/22/4/045005.

[46] L. Pentecoste *et al.*, “Low energy and low fluence helium implantations in tungsten: Molecular dynamics simulations and experiments,” *Journal of Nuclear Materials*, vol. 470, pp. 44–54, Mar. 2016, doi: 10.1016/j.jnucmat.2015.12.017.

[47] M. D. Hanwell, D. E. Curtis, D. C. Lonie, T. Vandermeersch, E. Zurek, and G. R. Hutchison, “Avogadro: an advanced semantic chemical editor,

visualization, and analysis platform," *J Cheminform*, vol. 4, no. 1, p. 17, Dec. 2012, doi: 10.1186/1758-2946-4-17.

[48] "Avogadro - Free cross-platform molecular editor," *Avogadro*. https://avogadro.cc/ (accessed Aug. 16, 2021).

[49] W. Humphrey, A. Dalke, and K. Schulten, "VMD: Visual molecular dynamics," *Journal of Molecular Graphics*, vol. 14, no. 1, pp. 33–38, Feb. 1996, doi: 10.1016/0263-7855(96)00018-5.

[50] "VMD - Visual Molecular Dynamics." http://www.ks.uiuc.edu/Research/vmd/ (accessed Aug. 16, 2021).

[51] W. Tian, W. Li, W. Yu, and X. Liu, "A Review on Lattice Defects in Graphene: Types, Generation, Effects and Regulation," *Micromachines*, vol. 8, no. 5, Art. no. 5, May 2017, doi: 10.3390/mi8050163.

[52] S. S. Roy, R. McCann, P. Papakonstantinou, P. Maguire, and J. A. McLaughlin, "The structure of amorphous carbon nitride films using a combined study of NEXAFS, XPS and Raman spectroscopies," *Thin Solid Films*, vol. 482, no. 1–2, pp. 145–150, Jun. 2005, doi: 10.1016/j.tsf.2004.11.132.

[53] A. Mueller, M. G. Schwab, N. Encinas, D. Vollmer, H. Sachdev, and K. Müllen, "Generation of nitrile groups on graphites in a nitrogen RF-plasma discharge," *Carbon*, vol. 84, pp. 426–433, Apr. 2015, doi: 10.1016/j.carbon.2014.11.054.

Table and Figure Captions

Fig 1 Snapshot of a typical simulation box filled with N_2 molecules. Carbon atoms in the 4.3x4.9 nm^2 graphene sheet are presented in cyan color in the middle of the image. Nitrogen atoms are presented with blue color

Fig 2 SEM images of: a) reference CNWs, b) nitrogen treated CNWs placed on the grounded electrode, and c) nitrogen treated CNWs placed on the powered electrode

Fig 3 a) XPS survey spectra of the reference and plasma treated CNWs. Core level high resolution C 1s region with corresponding fits for b) reference CNWs sample c) nitrogen treated CNWs placed on grounded electrode (GE) and d) nitrogen treated CNWs placed on powered electrode (PE). Core level high resolution N 1s region with corresponding fits for e) nitrogen treated CNWs placed on GE, and f) nitrogen treated CNWs placed on PE. O 1s region : g) nitrogen treated CNWs on GE, h) nitrogen treated CNWs on PE .

Fig 4 NEXAFS C K-edge spectra of the plasma functionalized CNWs: C1 sp^2 C=C, C2-C3 Rydberg peaks – graphene "fingerprint region", C4-C5 sp^3 C-C

Fig 5 NEXAFS N K-edge spectra of the plasma functionalized CNWs. Red line is showing spectra for the sample which was on the grounded electrode and the black line is showing spectra for the sample on the powered electrode

Fig 6 Snapshots of the graphene sheet modifications after 10^6 time steps

Fig 7 Type of defects observed in simulations a) vacancies, b) bridge nitrogen, c) on top N, d) pyridinic N, e) graphitic N, f) on top NH, g) amine. Free N_2 is appearing in f and g are not bound to the graphene sheet. The scheme is obtained by analyzing part of simulations by Avogadro and VMD software

Fig 8 Type and number of bonding situation at the end of MD simulation experiment for the nitrogen-based radicals interacting with graphene sheet

Fig 9 MD frames illustrate instabilities during the creation of graphitic-N defect. The time interval between two frames is 0.083 ps

Figures

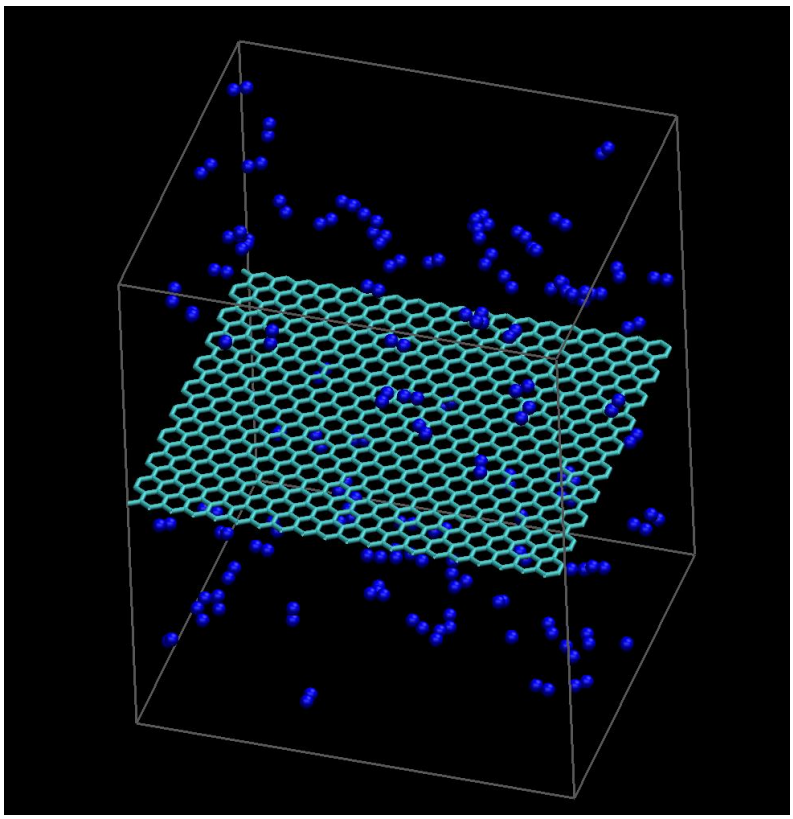

Fig 1

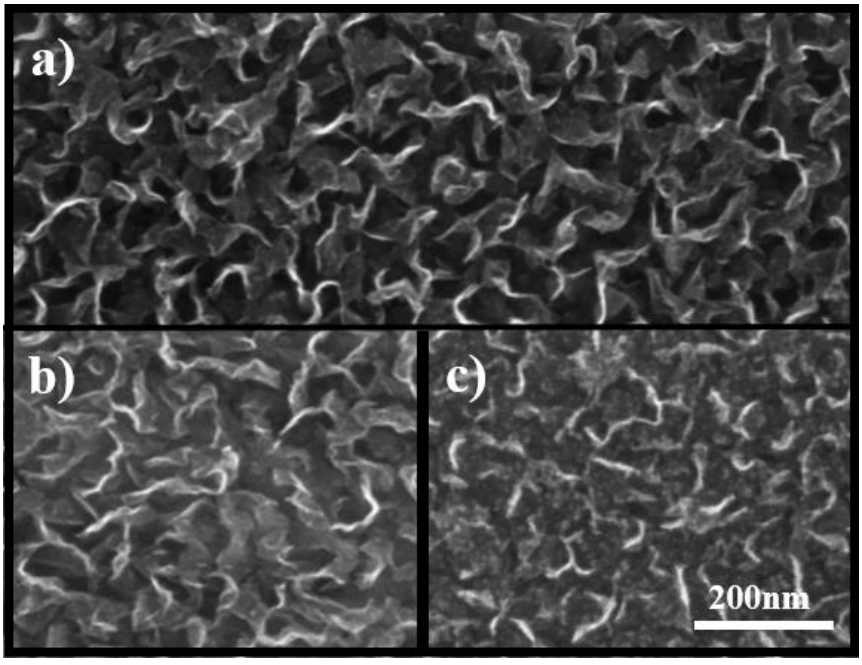

Fig 2

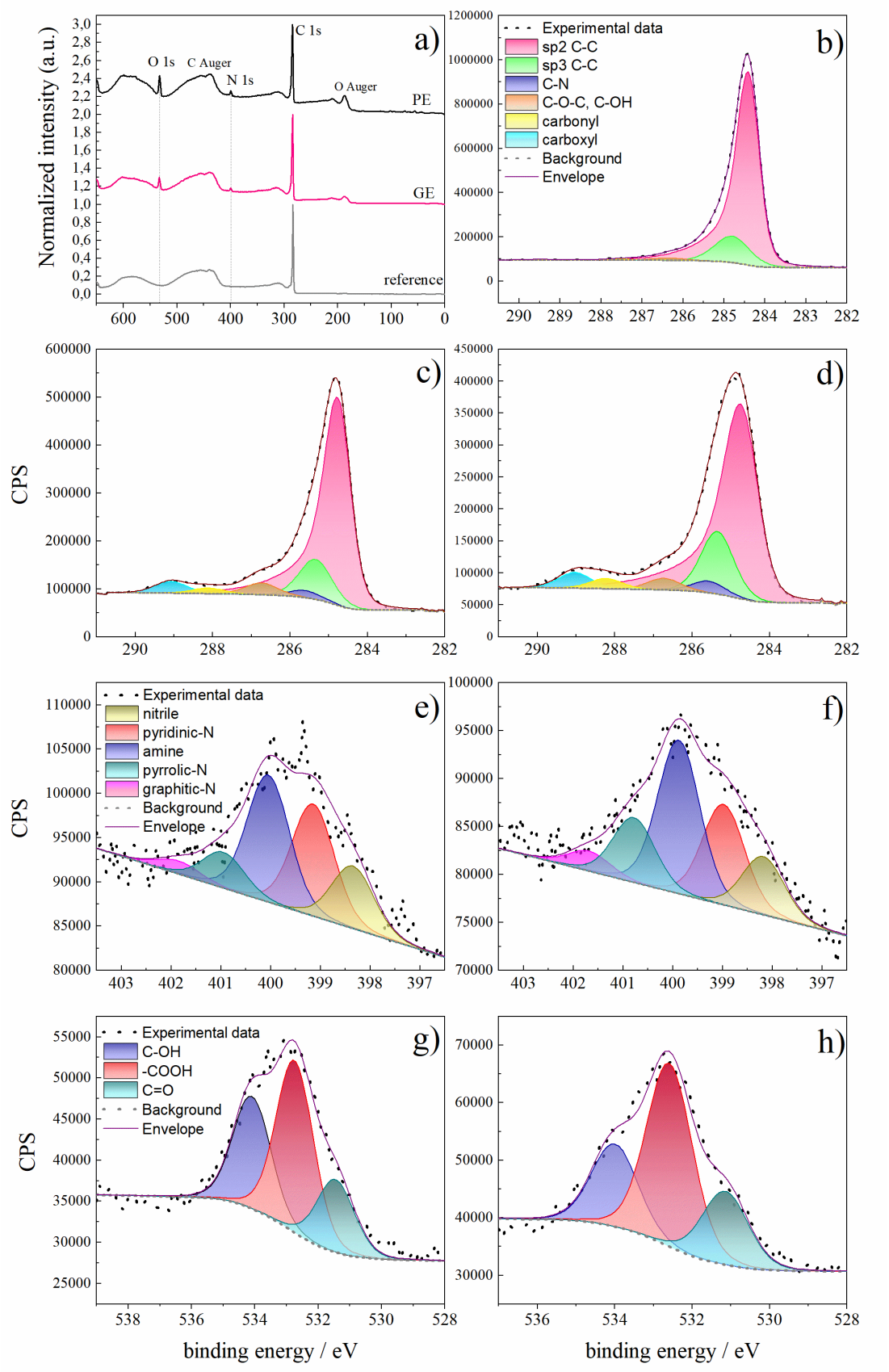
a)
Normalized intensity (a.u.)
C 1s
O 1s
C Auger
N 1s
O Auger
PE
GE
reference
b)
Experimental data
sp2 C-C
sp3 C-C
C-N
C-O-C, C-OH
carbonyl
carboxyl
Background
Envelope
c)
d)
CPS
e)
nitrile
pyridinic-N
amine
pyrrolic-N
graphitic-N
f)
g)
C-OH
-COOH
C=O
h)
binding energy / eV

Fig 3

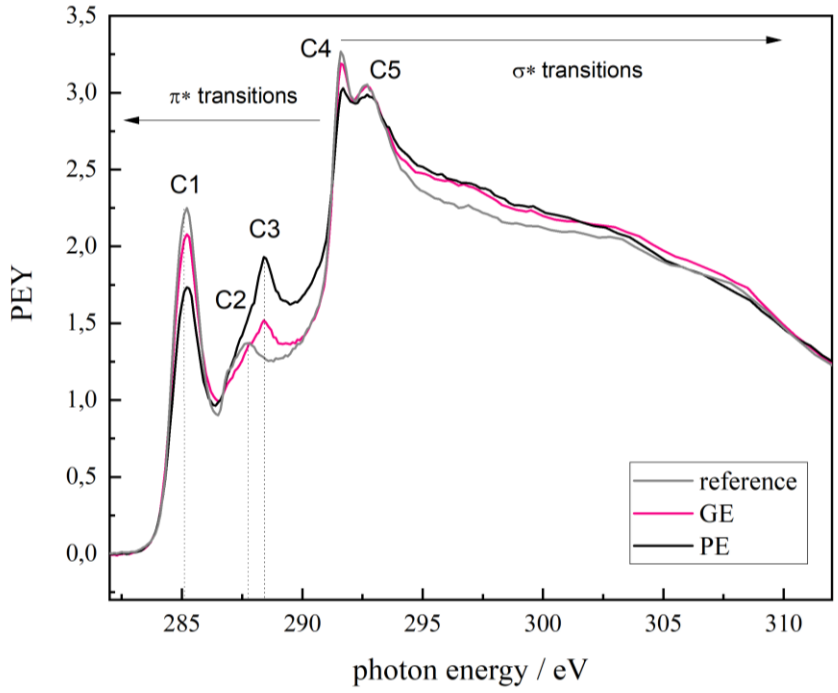
C4
C5
σ* transitions
π* transitions
C1
C3
C2
PEY
reference
GE
PE
3,5
3,0
2,5
2,0
1,5
1,0
0,5
0,0
285
290
295
300
305
310
photon energy / eV

Fig 4

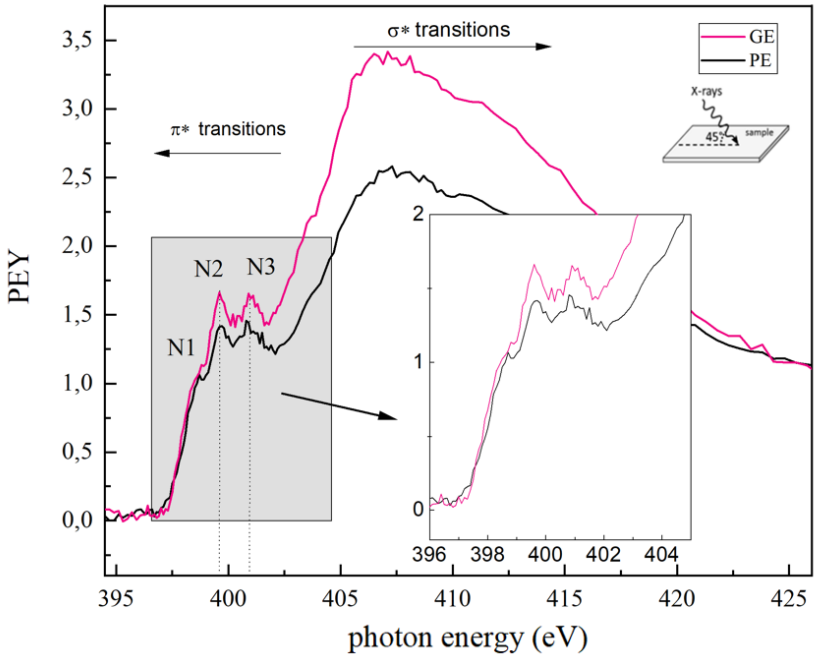
σ* transitions
GE
PE
X-rays
45°
sample
π* transitions
N2
N3
N1
PEY
2
1
0
396
398
400
402
404
3,5
3,0
2,5
2,0
1,5
1,0
0,5
0,0
395
400
405
410
415
420
425
photon energy (eV)

Fig 5

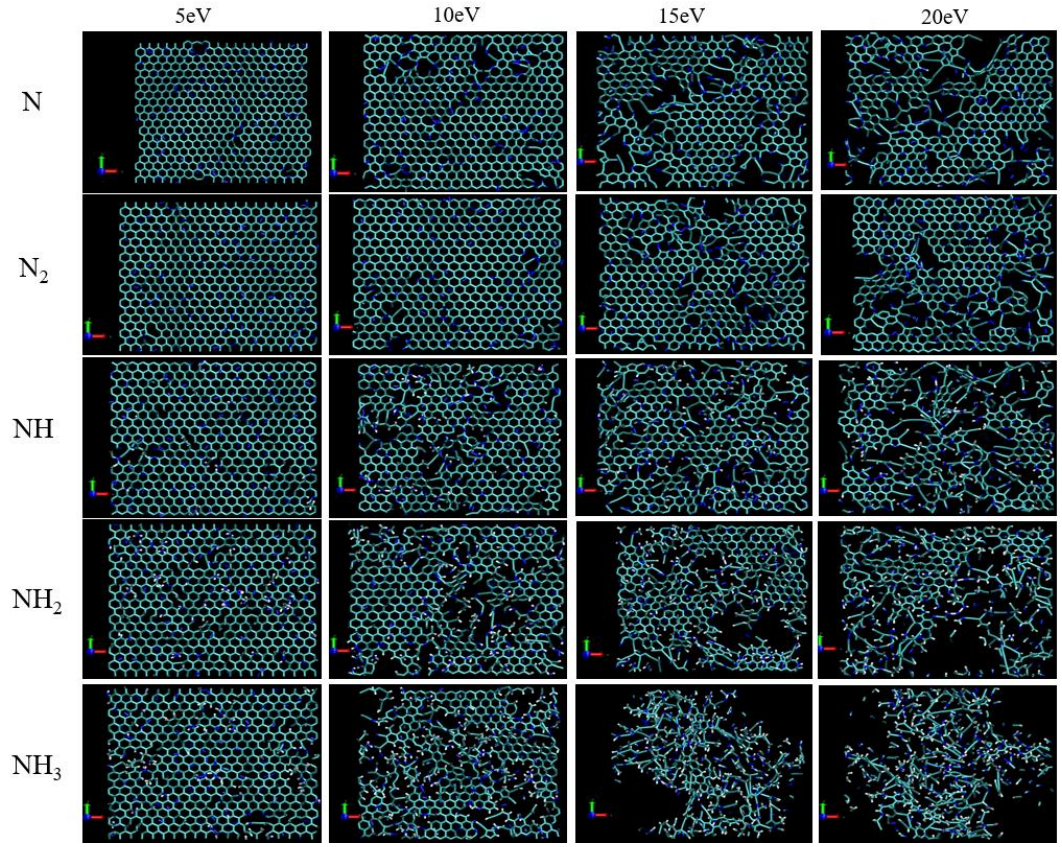

Fig 6

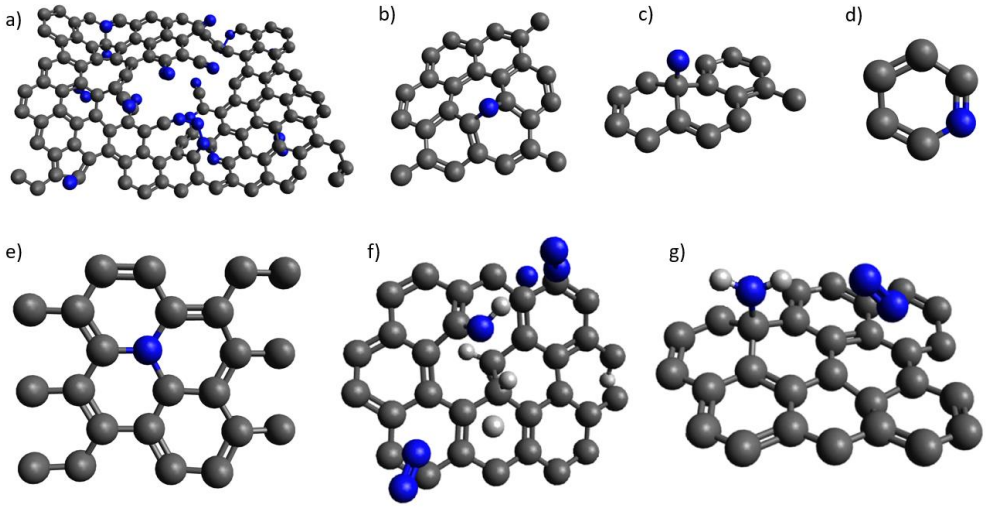

Fig 7.

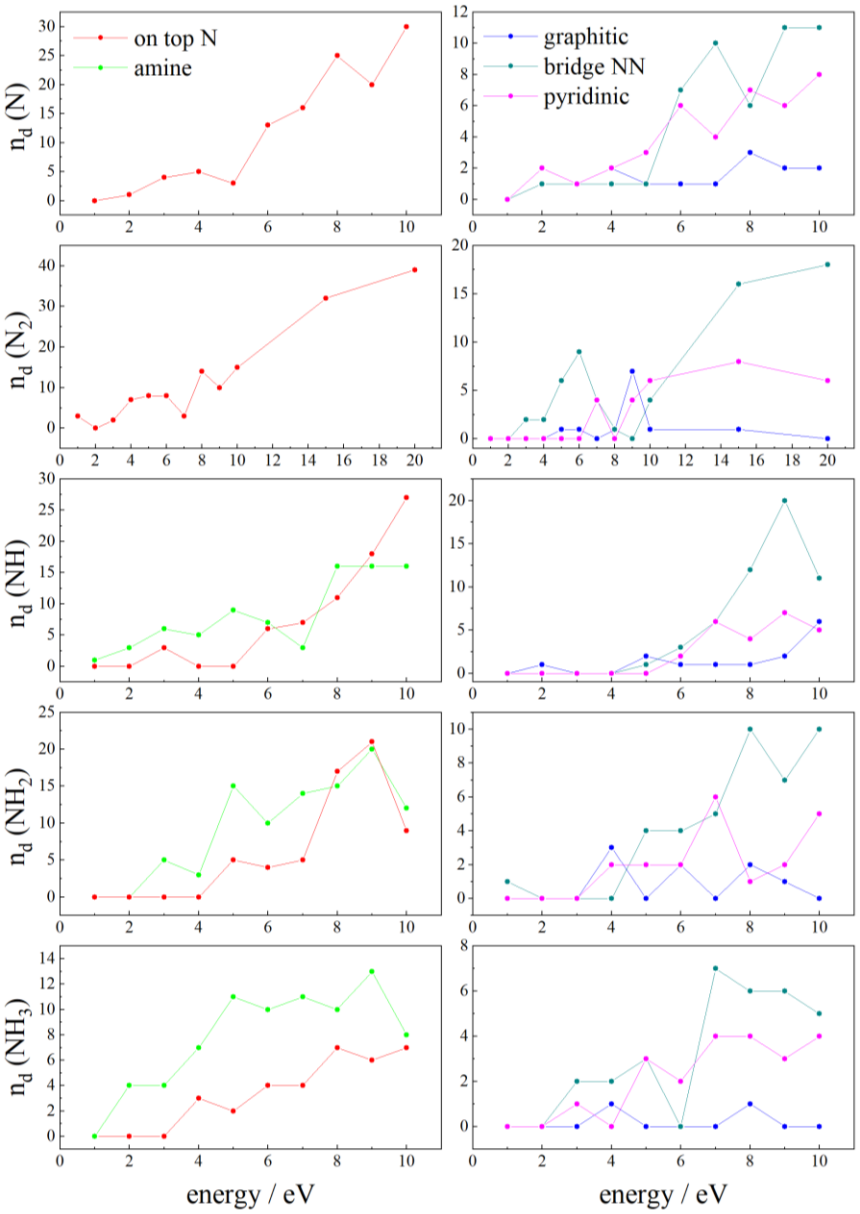
on top N
amine
graphitic
bridge NN
pyridinic
n_d (N)
n_d (N_2)
n_d (NH)
n_d (NH_2)
n_d (NH_3)
energy / eV
energy / eV

Fig 8

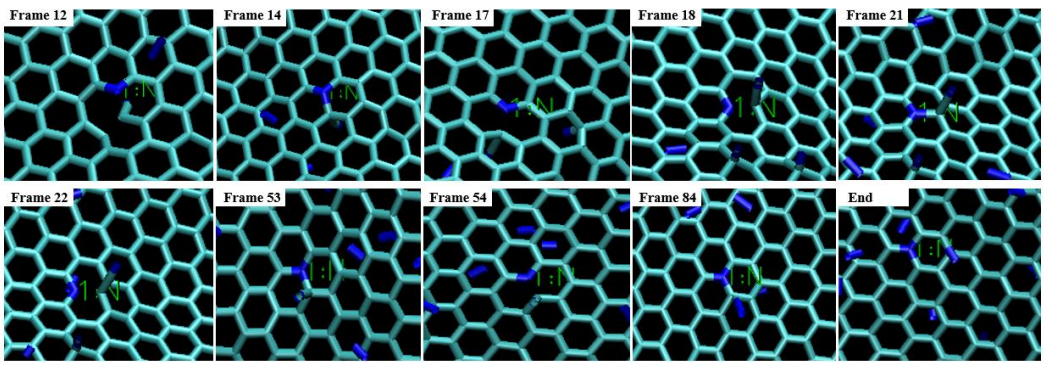
Frame 12
Frame 14
Frame 17
Frame 18
Frame 21
Frame 22
Frame 53
Frame 54
Frame 84
End

Fig 9